HHS Public Access

Author manuscript

Biochim Biophys Acta. Author manuscript; available in PMC 2019 February 01.

Published in final edited form as:

Biochim Biophys Acta. 2018 February ; 1866(2): 356–365. doi:10.1016/j.bbapap.2017.10.004.

PAK4 crystal structures suggest unusual kinase conformational movements

Eric Y. Zhang[1], **Byung Hak Ha**[2], and **Titus J. Boggon**[1,2,*]

[1]Department of Molecular Biophysics and Biochemistry, Yale University School of Medicine, 333 Cedar St., New Haven, CT 06520

[2]Department of Pharmacology, Yale University School of Medicine, 333 Cedar St., New Haven, CT 06520

Abstract

In order for protein kinases to exchange nucleotide they must open and close their catalytic cleft. These motions are associated with rotations of the N-lobe, predominantly around the 'hinge region'. We conducted an analysis of 28 crystal structures of the serine-threonine kinase, p21-activated kinase 4 (PAK4), including three newly determined structures in complex with staurosporine, FRAX486, and fasudil (HA-1077). We find an unusual motion between the N-lobe and C-lobe of PAK4 that manifests as a partial unwinding of helix αC. Principal component analysis of the crystal structures rationalizes these movements into three major states, and analysis of the kinase hydrophobic spines indicates concerted movements that create an accessible back pocket cavity. The conformational changes that we observe for PAK4 differ from previous descriptions of kinase motions, and although we observe these differences in crystal structures there is the possibility that the movements observed may suggest a diversity of kinase conformational changes associated with regulation.

Graphical abstract

*To whom correspondence should be addressed: Titus J. Boggon, Department of Pharmacology, Yale University School of Medicine, SHM B-316A, 333 Cedar St., New Haven, CT 06520, Phone: (203) 785-2943, Fax: (203) 785-5494, titus.boggon@yale.edu.

ACCESSION CODES

Crystallographic coordinates and structure factors have been deposited in the Protein Data Bank under accession codes: 5VED, 5VEE, 5VEF. X-ray diffraction images are available online at SBGrid Data Bank[42]: doi:10.15785/SBGRID/492 (5VED), doi:10.15785/SBGRID/493 (5VEE), doi:10.15785/SBGRID/494 (5VEF).

Declarations of interest. The authors declare no competing financial interests.

Author contributions. Performed the experiments: EYZ, BHH, TJB. Conceived and designed experiments: BHH, TJB. Analyzed the data: EYZ, TJB. Wrote the paper: EYZ, BHH, TJB.

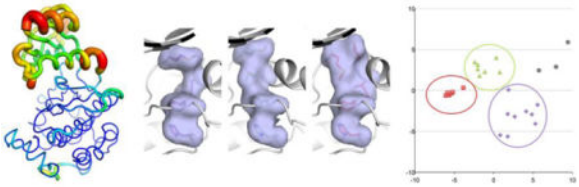

Keywords

Crystal structure; Kinase conformation; Protein structure; Inhibitor design; Gatekeeper; Back pocket

INTRODUCTION

Conformational movements in protein kinases are important for regulation of these important signaling proteins. The protein kinase fold consists of two lobes (N- and C-) which clasp ATP in a deep cleft between them. When phosphotransfer is complete, the resulting ADP molecule is released and a new ATP molecule bound. This release and binding of nucleotide is thought to be associated with a ‘hinge’ motion between the N- and C-lobes[1]. Most analysis for this motion has been conducted for the archetypal PKA, and suggests both a shear/pivot of the N-lobe and a conformational movement in a loop termed the glycine-rich-loop, are important for nucleotide cycling and kinase activity regulation[1–4], however, kinase regulation is conformationally diverse, and there is the potential that these PKA motions may not readily describe the whole kinase group.

The p21-activated kinases (PAKs) are downstream effectors of Rho small GTPases and are important for cell proliferation, survival, motility, and angiogenesis[5]. PAK4, PAK5 and PAK6 comprise the type II sub-group and regulate key cellular substrates involved in regulation of actin cytoskeleton structure and adhesion, including the LIMK, GEFH1, integrin β5, β-catenin and paxillin[6]. These serine-threonine kinases are usually thought to be constitutively phosphorylated on their activation loop[7, 8], and GTPase binding is thought to be important for kinase targeting but not direct activation, at least for PAK4[9–11], although caveats to these observations may exist in the cellular context[9]. Nonetheless, regulation of kinase activity for the type II PAKs is thought to be achieved by non-canonical means, predominantly by interactions of the phosphorylated kinase with pseudosubstrate motifs[10, 12, 13], although a complete understanding of activity regulation is yet to be achieved.

Type II PAKs are drivers of oncogenic Rho-GTPase signaling, and their amplification and dysregulated activity have been implicated in a range of cancers including colorectal, breast, and pancreatic[5, 6]. The PAKs in general, and PAK4 in particular, are therefore thought to hold promise as targets for small molecule therapeutics[6, 14, 15]. Multiple compounds have been developed to target PAK4[16], but selectivity across the group has been difficult to achieve, for example, PF-3758309 which went to clinical trials, has only limited selectivity between the type I and type II PAKs[16]. To improve this, targeting a large hydrophobic pocket adjacent to the catalytic cleft, which is sometimes observable in type II PAK crystal

structures, has been proposed, and demonstrated[17]. Many small molecule inhibitors bind a specific kinase conformation[18] and inform on the natural conformational variability accessible to the kinase. Therefore, for the type II PAKs the ability to target a large hydrophobic pocket located directly beside the catalytic cleft represents a potentially unusual state that occurs in the kinase's normal repertoire of conformations.

In this study we have determined three co-crystal structures of PAK4 with small molecule inhibitors from different scaffold classes, the large pan-specific inhibitor staurosporine, the Rho kinase inhibitor fasudil (HA-1077), and FRAX486, a compound which rescues Fragile X phenotypes in the *Fmr1* knockout mouse[19]. We analyze these structures in the context of all previously published PAK4 structures. Using principal component analysis of the crystal structures we find that PAK4 structures can be classified into distinct conformational groups, and that these groups are associated with specific orientations of helix αA, αC, and the hydrophobic kinase regulatory spine. Our study implies a diversity of conformational movements for protein kinases.

RESULTS

Overall structures of PAK4 in complex with staurosporine, fasudil and FRAX486

We determined the co-crystal structures of PAK4 in complex with staurosporine, fasudil, and FRAX486. The structures are in the same space group ($P4_12_12$) with similar unit cell parameters (Table 1) and were determined to 2.3 Å, 1.75 Å and 2.5 Å resolution (for the staurosporine, fasudil, and FRAX486 complexes, respectively). Each structure displays the typical bi-lobed kinase fold, with a β-sheet dominated N-lobe and an α-helical dominated C-lobe. Juxtaposed between the lobes is the catalytic cleft that normally binds ATP, and in each of the structures binds to the inhibitor in an ATP-competitive manner. The electron densities of the small molecule inhibitors allow a clear definition of their pose (Figs 1, S1). As found in all other structures of PAK4, the protein is phosphorylated on the activation loop (residue pSer474) and the kinase is observed in the active, DFG-in, conformation.

Inhibitor poses in the catalytic cleft of PAK4

Staurosporine - The 2.3 Å co-crystal structure of PAK4 with staurosporine recapitulates a typical pose for staurosporine compared to 66 kinase-staurosporine co-crystal structures in the PDB (Figs 1A, S2A). It shows an ATP-competitive mode of binding characterized by hydrogen bonds between the O5 oxygen atom and the backbone nitrogen of Leu398, the N1 nitrogen atom and the backbone carbonyl of Glu396, and the N4 nitrogen atom with the backbone carbonyl of Asp444 (Fig 1D,G).

Fasudil - The 1.75 Å co-crystal structure of fasudil in complex with PAK4 shows the small molecule located in the catalytic cleft in an ATP-competitive pose (Fig 1B). The structure recapitulates some of the binding properties observed in the five previous crystal structures of kinases in complex with fasudil, of ROCK1, ROCK2, MRCKα and PKA [20–24]. In the PAK4-bound structure we observe that fasudil hydrogen bonds between its isoquinoline nitrogen and the backbone nitrogen of PAK4 Leu398, however, the presence of only a single hydrogen bond (Fig 1E,H) contrasts with the two or three observed in previous fasudil-

kinase complexes. Furthermore, PAK4 does not contain the phenylalanine residue conserved in the C-terminal tail of the AGC kinases (Phe327 in PKA; Phe368 in ROCK1). This phenylalanine inserts into the ATP pocket from the C-terminal tail of the kinase and makes hydrophobic contact with fasudil[20–24]. In the AGC kinase family structures Phe327/Phe368 packs against fasudil to push it deep into the catalytic cleft. An equivalent residue is not contained in PAK4, consequently the isoquinoline ring of fasudil is displaced outwards by up to 2 Å compared to the ROCK or PKA structures (Fig S2B). In PAK4-fasudil, the seven-membered isoquinoline ring also adopts a slightly different skew than observed in the AGC kinase structures. The other major component of the small molecule, the homopiperazine ring, can adopt two different conformations in AGC kinase-bound structures, one is rotated closer to the glycine-rich loop, and a second rotated closer to the hinge region[22] (Fig S2C). In the PAK4 bound structure the homopiperazine ring displays poor electron density and higher *B*-factor, illustrating its flexibility, but is predominantly located in the glycine-rich loop proximal conformation (Figs 1E, S2C).

FRAX486 - The 2.5 Å structure of FRAX486 with PAK4 is the first reported co-crystal structure of a type II PAK in complex with a compound containing a pyrido[2,3-*d*]pyrimidine-7-one core, from a series developed by Afraxis[16, 25, 26]. The molecule is located in the catalytic cleft (Fig 1C) and stabilized by a two hydrogen bonds between to the carbonyl oxygen and backbone nitrogen of hinge residue Leu398 (Fig 1I). A 2,4-di-Cl-phenyl ring places the halide atoms abutting the gatekeeper residue Met395 and the VAIK motif Lys350 (Fig 1F,I). Three compounds based on the pyrido[2,3-*d*]pyrimidine-7-one core have previously been determined in complex with PAK1 (FRAX597, PDB ID: 4EQC[25]; FRAX1036, PDB ID: 5DFP[27]; G-5555, PDB ID: 5DEY[27]), and the pose of the small molecule core is similar in each (Fig S2D). FRAX486 displays selectivity for PAK1 over PAK4 (IC_{50} PAK1, 8 nM; IC_{50} PAK4, 779 nM), and it has been hypothesized that pyrido[2,3-*d*]pyrimidine-7-one selectivity comes from the conformational preferences of the gatekeeper residue (Met395 in PAK4, Met344 in PAK1) and the VAIK motif lysine (Lys350 in PAK4, Lys299 in PAK1)[16]. This is difficult discern from comparison of our structure with the PAK1 structures, particularly as two of those are for kinase inactivating VAIK motif K→R mutant proteins (PDB IDs: 4EQC, 5DFP).

Assessment of conformational orientation of PAK4

Including the three described here, there are 28 deposited crystal structures of the catalytic domain of PAK4. We hypothesized that these structures should allow a better understanding of the conformational diversity accessible to PAK4 so we began by conducting structural superpositions. This illustrated two common themes of kinase structure, the stable conformation of the α-helical C-lobe and movement of the β-strand-rich N-lobe with respect to the C-lobe (Fig 2A). The three structures that we have determined fit broadly into the range of conformational movement found in previous PAK4 structures (Fig 2A). However, on closer examination of root-mean-square deviations (RMSD) between the structures, we find potentially interesting conformational changes, particularly in the region of helix αC (Fig 2B,C). We therefore conducted a cross correlation analysis where we observe some positive correlations, (e.g. between the regions of the helix αC and the DFG-motif). As expected, we also observe that the N-lobe as a whole seems to act as a correlated unit

disunited with the rest of the kinase domain. The N-lobe shows positive correlation with itself (Fig 2D, blue, approximate residues 300–400), and weak positive correlation with the C-terminal portion of the domain comprising helices αF, αG and αI (Fig 2D, approximate residues 500–575), it also shows negative correlation with the middle third of the domain comprising αD through αF and representing the middle layer of the domain (Fig 2D, approximate residues 400–500). Because some regions within the N-lobe have conformational differences that are more tightly correlated to one another compared to the rest of the catalytic domain (Fig 2D), we conducted further analysis of the PAK4 N-lobes.

Assessment of conformational orientation of the N-lobe of PAK4

We superposed the N-lobes of the PAK4 structures and observed that while there is much conformational stability over the structures (Fig 3A), three regions have increased flexibility. The first is the N-terminal helix, helix αA, (residues ~301–307), a helix not conserved in the canonical protein kinase fold, but in a location often important in kinase regulation. The second is at the tip of the glycine-rich loop (residues 330–332), particularly for the backbone of residue Ser331. Glycine-rich loop movements are canonically associated with nucleotide binding and release[4], and with altered kinase conformations on inhibitor binding[28]. The third region of conformational variance between the structures is at the C-terminus of the C-helix (residues ~366–374). These ‘by-eye’ observations were confirmed by RMSD analysis (Fig 3B,C). We next asked if these movements were correlated with one another. Cross correlation analysis for the N-lobe alone showed positive correlation between helix αA, and the β2-β3 and β3-αC loops (Fig 3D), between the VAIK motif (in β3) and the GxGxxG motif (β1-β2 loop), and negative correlations between the β2-β3, β1 and β4. Since these correlations suggested concerted movements in the kinase N-lobe, we conducted further *in silico* analyses of the PAK4 structures.

Principal Component Analysis

The PAK4 structures display diversity in their conformations, but the above analyses suggest that correlations may exist between specific regions that contribute to the shape of the catalytic cleft. To better understand these correlations, we conducted Principal Component Analysis (PCA) for the PAK4 structures. PCA is widely used as a technique to reduce multi-dimensional data by linear transformation in order to describe the variance among a set of data, and for macromolecular structures yields eigenvectors that most parsimoniously separate the structures based on conformational changes, to allow rational structure-based conformational classification. The vector that describes the maximal spread of the data is termed principal component 1 (PC1), the second most variable vector is PC2, etc[29]. Although for macromolecular structures PCA is often used to analyze molecular dynamics simulations or NMR ensembles, there are now multiple studies that treat crystal structures of the same protein as an ensemble of conformations, thus allowing informative PCA based on crystallographic data[30–33]. Overall, for the PAK4 kinase domain we find that the first principal component explains 36% of the motions, the second 28% and the third 13%. The first three PCs therefore describe 76% of motions between the structures (Fig S3A). For the N-lobe alone (residues 301–399) we find that the first principal component explains 38% of the motions, the second 15% and the third 11%, accounting for 65% of motions (Fig 4A). We conducted two-dimensional mapping for the first three principal components (Fig 4B,

S3B), and analyzed the contribution of each residue to each principal component (Fig 4C, S3C). Predictably, for the catalytic domain as a whole the conformational movements of the N-lobe dominate the analysis (Fig S3C). However, for the N-lobe, the by-residue analysis (Fig 4C) indicates that much of the differences between conformations are derived from different alternate states in and around helix αC (residues 366–372), with Met370 providing the biggest single contribution to PC1 (Fig 4C). Clustering of the structures based on the PC1–PC2 principal component analysis for the N-lobe suggests four groups (Fig 4D), which we interpret to represent different classes of N-lobe conformation.

Clustering of PAK4 conformations

The PCA clustering analysis indicates four groups that are broadly associated with conformational movements of the N-lobe. When the structures are superposed on the core residues and colored by group, the conformational differences between the clusters become apparent (Fig S4A). The groups can be classified to (1) an ATP-bound-like conformation (in green; PDBs: 2CDZ, 2Q0N, 4FIE, 4FIF, 4FIG, 4XBR, 5BMS), (2) a substrate-bound-like conformation (in red; PDBs: 4FIH, 4FII, 4FIJ, 4JDH, 4JDI, 4JDJ, 4JDK, fasudil), (3) inhibitor-accessible-only conformations (in grey; PDBs: 2X4Z, 4APP, FRAX486), and (4) a conformation that opens up a back pocket cavity behind the gatekeeper residue (in purple; PDBs: 2J0I, 4L67, 4NJD, 4O0V, 4O0X, 4O0Y, 4XBU, 5IOB, staurosporine).

The ATP-bound-like, substrate-bound-like and back-pocket cavity-associated conformations each display typical poses unique to their group; in contrast, the inhibitor-accessible-only conformations don’t easily fall into a common conformation. The differences between the ATP-bound-like, substrate-bound-like and back-pocket cavity-associated groups are highlighted by a conformational movement at the C-terminus of helix αC, which in the context of the whole molecule manifest as a solenoid-like movement of helix αC of approximately 3–4 Å (Fig S4B). At the side-chain level this movement is associated with a series of rearrangements of the van der Waals interactions between helix αC, the β4 strand and the DFG motif/activation loop. Specific residues are particularly affected: Phe459 and Cys462 in the DFG-motif/activation loop, Ile369 and Met370 in helix αC, and Met381 in the β4 strand (Fig S4C). Comparison of just the substrate-bound-like and ATP-bound-like states indicate that substrate binding might be associated with a more closed N-lobe orientation which results in more rigid placement of multiple residues including helix αC residues Arg371 and Phe364, helix αA residues Leu308 and F304, and residues of the β3-αC loop (Fig S4D)

Rigid core analysis

To investigate the basis for differences between the conformational clusters, we conducted rigid core discovery for both the whole kinase domain and the N-lobe, based on root-mean-square deviations of carbon alpha atoms. We find that for the N-lobe alone the rigid core is comprised of the β-sheet (Fig 5A) but for the whole kinase domain the core encompasses much of the C-lobe and an additional three residues in the N-lobe (Asn377, Val378, Val379) between helix αC and β4 (Fig 5B). Movement of the N-lobe with respect to the C-lobe do not affect residues in the canonical hinge region (beginning at Glu399) or at the tip of the αC-β4 loop. Therefore, movements of the N-lobe seem to create stresses within the kinase

domain that are relieved conformationally, particularly at the C-terminal region of helix αC where there is an unwinding of the final helical turn (Fig 5C).

Hydrophobic spine rearrangement

A major impact of these hinge movements is on the orientation of the kinase hydrophobic spines. For protein kinases two hydrophobic clusters of side-chains are thought to play important roles in orienting residues for catalysis and regulation[3, 34, 35]. These two 'hydrophobic spines' are termed the C-spine and the R-spine. We observe few changes in the C-spine between PAK4 structures, however, there are significant changes in the PAK4 R-spine (regulatory spine), the positions of which are termed RS1-RS4 [3]. In each state, the RS1 and RS2 positions are occupied by His438 and Phe549, respectively (Fig 6A). However, the RS3 and RS4 positions are labile. The ATP-bound-like state is a canonical R-spine with Met370 taking the RS3 position and Met381 taking the RS4 position. In contrast, in the substrate-bound-like state the RS3 position is occupied by two residues, Ile369 and Met381, and RS4 by Met370. The back-pocket-accessible conformation is different again, and displays a degraded R-spine with RS3 (Met370) making poor contacts with RS4 (Met381). There seems to be a pathway of movement between these classes of structure for residues in the RS3 and RS4 positions and also outside of the R-spine (Fig 6B). The PCA analysis therefore seems to indicate that the PAK4 structures have captured a trajectory of conformational states (Fig 6C) that describe accessible conformations for the kinase, ranging from a back-pocket-accessible inactive state, through a canonical conformation for a ATP-bound kinase domain, to an „in the act‟ kinase state typified by an unusual conformation of the R-spine.

Discussion of the influence of crystal packing

Crystal structures can be subject to induced fit from crystal packing effects. As these can be associated with conformational changes we analyzed the packing of the structures. 19 of the PAK4 crystal structures are in the same crystal form with space group $P4_12_12$ and unit cell parameters of a=b ≈ 63 Å, c ≈ 182 Å. All four classes are found in this form: (5BMS), (2J0I, 4L67, 4NJD, 4O0V, 4O0X, 4O0Y, 4XBU, 5I0B, staurosporine), (FRAX486), (4FIH, 4FII, 4FIJ, 4JDH, 4JDI, 4JDJ, 4JDK, fasudil). So, although the substrate-bound-like and back-pocket cavity-associated conformations are only observed in this space group, the variety of conformations suggest a wide range of conformational accessibility. Induced fit also has the possibility to prevent canonical reorientation of helix αC, perhaps by an interaction between the N-lobe of PAK4 and an adjacent molecule. This interaction does occur in the $P4_12_12$ crystal form, potentially impacting the orientation of the C-lobe, however, we note that an array of small molecule inhibitors have been rationally designed to target the back pocket of PAK4[17, 36, 37]. The ability of these small molecule inhibitors to bind the back pocket accessible conformation shows that this conformation does occur in solution. Additionally, similar crystallization conditions can yield multiple classes (Table S1). Therefore, the conformational differences we observe between the structures may not be unduly influenced by crystal packing effects.

DISCUSSION

PAK4 is now a well-studied protein kinase, with crystal structures solved in various space groups and in complex with an array of small molecule inhibitors, peptide substrates, pseudosubstrates, and nucleotide. This has allowed us to conduct a detailed study of the conformational accessibility of PAK4 in the crystalline environment. We find that the movements of the N-lobe of PAK4 are unusual and seem to create torsional stresses that are previously undescribed in protein kinases and manifest in partial unwinding of helix αC. Our principal component analysis allowed us to rationalize these observed in crystal differences into three major states which broadly cluster with different orientations of a region of the kinase hydrophobic core, known as the 'R-spine'[3, 34, 35]. In particular, movements in the R-spine RS3 and RS4 positions are associated with unwinding of helix αC. Notably, this degradation of the R-spine creates an accessible back pocket cavity behind the kinase gatekeeper residue which can be targeted by small molecule inhibitors[17]. We note that a comparison of R-spines for staurosporine-bound kinases (Fig S5) shows that three structures of CDK2 (1aq1, 4erw and 4ez7)[38, 39] have disrupted R-spines that create a pocket accessible for allosteric inhibitors[38], illustrating the potential of this region for targeting PAK4.

PAK4 is thought to be predominantly constitutively phosphorylated on its activation loop in the cell[7, 8, 40]. Its regulation has therefore has been proposed to be restricted to pseudosubstrate autoinhibition of the active-conformation kinase[7, 10]. Recently, a protein inhibitor of PAK4 was discovered (called Inka1, PDB ID: 4XBU) and this is thought to use a similar pseudosubstrate-like mechanism to inhibit kinase activity[41]. Our analyses find that the Inka1-bound state, and also an autoinhibited conformation bound to a long pseudosubstrate peptide (PDB ID: 4L67), both cluster in the degraded R-spine group. It is attractive therefore to postulate that the back-pocket-accessible conformation arises from additional structural changes to achieve complete restriction of catalytic activity. We propose this to be a previously unrecognized inactive PAK4 conformation.

Protein kinases must open and close their catalytic cleft to allow binding and release of nucleotide. These motions are associated with rotations of the N-lobe around the 'hinge region' [1], a second region at the N-terminus of β4[2] and conformational flexibility in the glycine-rich loop[4]. Although these observations were made for PKA, they are thought to apply across the family. The conformational changes that we observe in our study of 28 PAK4 crystal structures differ from these previous observations, particularly in the movements of helix αC, therefore our findings potentially support a diversity of kinase conformational changes associated with regulation.

Materials and Methods

Protein expression and purification

Expression and purification of PAK4 catalytic domain has been previously described[10, 43]. Briefly, the catalytic domain of PAK4 (UniProt ID O96013-2) was expressed from a modified pET28 vector with a hexa-histidine (6xHis) tag which was removable by TEV protease. Following Ni-affinity HisTrap chelating column (GE Healthcare) chromatography,

anion Exchange Resource S (GE Healthcare), and gel filtration Superdex 200 10/300GL (GE Healthcare) the purified PAK4 catalytic domain was concentrated to 4 mg/ml for co-crystallization.

Co-crystallization

Small molecule inhibitors fasudil (HA-1077) (Cayman Chemical), staurosporine (LC Laboratories) and FRAX486 (Selleck Chemicals) were purchased and resuspended in DMSO to concentrations of 5.5 mM, 20 mM and 100 mM respectively. The inhibitors were mixed in 1:1 volume ratios with PAK4 and co-crystallization trials set up using hanging drop vapor diffusion methodology. Optimized crystallization conditions for PAK4-cat were obtained at 0.1 M Tris-HCl (pH 7.5) and 1.5 – 2.0 M Na acetate at room temperature. Before flash-freezing in liquid nitrogen, the crystals were equilibrated using 2.5 M sodium acetate as cryoprotectant.

Data collection and structure determination

X-ray diffraction data were collected at beamline 24-ID-E, Northeastern Collaborative Access Team facility (NE-CAT), at Argonne National Laboratory. Integration and scaling were performed using the HKL2000 package[44], and initial phases obtained using Phaser[45] with a search for the PAK4 catalytic domain (PDB ID: 4FIJ[10]) yielding TFZ scores of 10.3, 8.5 and 65.3 for the FRAX486, staurosporine and fasudil-bound structures respectively. The PAK4 protein components of the structures were refined using Phenix[46] or Refmac[47] and model building performed using Coot[48]. Once extensive difference density became visible in the catalytic cleft coordinates for the small molecules were manually docked and refined. PDB coordinates and cif files for fasudil and staurosporine were downloaded from the RCSB PDB website (www.rcsb.org), and generated for FRAX486 using the PRODRG server[49]. The final structures show good model quality as assessed by MolProbity [50] (Table 1). Crystallographic software compiled by SBGrid[51], structural figures generated using CCP4mg [52] and PyMOL (Schrödinger, LLC).

Structure analyses, including PCA

The following crystal structures of PAK4 were used in the analysis: 2CDZ, 2J0I [53], 2Q0N, 4JDH, 4JDI, 4JDJ, 4JDK [43], 2X4Z [54], 4APP [55], 4FIE, 4FIF, 4FIG, 4FIH, 4FII, 4FIJ [10], 4L67 [12], 4NJD [36], 4O0V, 4O0X, 4O0Y [17], 4XBR, 4XBU [41], 5BMS [56], 5I0B [37]. Analyses did not include 2BVA [53] because of excessive missing residues in that structure. Primary amino acid sequences for each peptide chain were extracted using Moleman2[57], aligned using Muscle[58] and maximum likelihood superposition and cross correlations calculated using Theseus[59]. Analysis included chain A for structures with two highly similar chains. For whole kinase domain analysis, all residues before His301 and after Arg589 were removed from the PDB files, for N-lobe analysis all residues before His301 and after Glu399 were removed from the PDB files. Rigid core identification was conducted using the core.find() command in Bio3d[60] and for the whole kinase comprised residues 377–379, 400–434, 436–449, 452–457, 459, 462, 471–473, 475–487, 491–516, 518, 523–527, 530–533, 535 and 542–586. For the N–lobe the rigid core comprised residues 312–328, 333–341, 345–354 and 379–398. Per residue RMSD was calculated using

Theseus. Principal component analysis was conducted using Bio3d with the pca.xyz() command. PCA dendrograms were generated using the hclustplot() command.

Supplementary Material

Refer to Web version on PubMed Central for supplementary material.

Acknowledgments

We thank Amy Stiegler and Ben Turk for comments on the manuscript. APS beamline NE-CAT (24-ID-E and -C) is thanked and is funded by NIH grants GM103403 and RR029205. This work was funded by National Institutes of Health grant R01GM102262 and by S10OD018007.

References

1. Narayana N, Cox S, Nguyen-huu X, Ten Eyck LF, Taylor SS. A binary complex of the catalytic subunit of cAMP-dependent protein kinase and adenosine further defines conformational flexibility. Structure. 1997; 5:921–935. [PubMed: 9261084]
2. Tsigelny I, Greenberg JP, Cox S, Nichols WL, Taylor SS, Ten Eyck LF. 600 ps molecular dynamics reveals stable substructures and flexible hinge points in cAMP dependent protein kinase. Biopolymers. 1999; 50:513–524. [PubMed: 10479734]
3. Kornev AP, Taylor SS. Dynamics-Driven Allostery in Protein Kinases. Trends Biochem Sci. 2015; 40:628–647. [PubMed: 26481499]
4. Taylor SS, Yang J, Wu J, Haste NM, Radzio-Andzelm E, Anand G. PKA: a portrait of protein kinase dynamics. Biochim Biophys Acta. 2004; 1697:259–269. [PubMed: 15023366]
5. Arias-Romero LE, Chernoff J. A tale of two Paks. Biol Cell. 2008; 100:97–108. [PubMed: 18199048]
6. Radu M, Semenova G, Kosoff R, Chernoff J. PAK signalling during the development and progression of cancer. Nat Rev Cancer. 2014; 14:13–25. [PubMed: 24505617]
7. Ha BH, Morse EM, Turk BE, Boggon TJ. Signaling, Regulation, and Specificity of the Type II p21-activated Kinases. J Biol Chem. 2015; 290:12975–12983. [PubMed: 25855792]
8. Pandey A, Dan I, Kristiansen TZ, Watanabe NM, Voldby J, Kajikawa E, Khosravi-Far R, Blagoev B, Mann M. Cloning and characterization of PAK5, a novel member of mammalian p21-activated kinase-II subfamily that is predominantly expressed in brain. Oncogene. 2002; 21:3939–3948. [PubMed: 12032833]
9. Baskaran Y, Ng YW, Selamat W, Ling FT, Manser E. Group I and II mammalian PAKs have different modes of activation by Cdc42. EMBO Rep. 2012; 13:653–659. [PubMed: 22653441]
10. Ha BH, Davis MJ, Chen C, Lou HJ, Gao J, Zhang R, Krauthammer M, Halaban R, Schlessinger J, Turk BE, Boggon TJ. Type II p21-activated kinases (PAKs) are regulated by an autoinhibitory pseudosubstrate. Proc Natl Acad Sci U S A. 2012; 109:16107–16112. [PubMed: 22988085]
11. Tabanifar B, Zhao Z, Manser E. PAK5 is auto-activated by a central domain that promotes kinase oligomerization. Biochem J. 2016; 473:1777–1789. [PubMed: 27095851]
12. Wang W, Lim L, Baskaran Y, Manser E, Song J. NMR binding and crystal structure reveal that intrinsically-unstructured regulatory domain auto-inhibits PAK4 by a mechanism different from that of PAK1. Biochem Biophys Res Commun. 2013; 438:169–174. [PubMed: 23876315]
13. Gao J, Ha BH, Lou HJ, M ME, Zhang R, Calderwood DA, Turk BE, Boggon TJ. Substrate and inhibitor specificity of the type II p21-activated kinase, PAK6. PLoS One. 2013; 8:e77818. [PubMed: 24204982]
14. Eswaran J, Soundararajan M, Knapp S. Targeting group II PAKs in cancer and metastasis. Cancer Metastasis Rev. 2009; 28:209–217. [PubMed: 19160016]
15. King H, Nicholas NS, Wells CM. Role of p-21-activated kinases in cancer progression. Int Rev Cell Mol Biol. 2014; 309:347–387. [PubMed: 24529727]

16. Rudolph J, Crawford JJ, Hoeflich KP, Wang W. Inhibitors of p21-activated kinases (PAKs). J Med Chem. 2015; 58:111–129. [PubMed: 25415869]

17. Staben ST, Feng JA, Lyle K, Belvin M, Boggs J, Burch JD, Chua CC, Cui H, DiPasquale AG, Friedman LS, Heise C, Koeppen H, Kotey A, Mintzer R, Oh A, Roberts DA, Rouge L, Rudolph J, Tam C, Wang W, Xiao Y, Young A, Zhang Y, Hoeflich KP. Back pocket flexibility provides group II p21-activated kinase (PAK) selectivity for type I 1/2 kinase inhibitors. J Med Chem. 2014; 57:1033–1045. [PubMed: 24432870]

18. Muller S, Chaikuad A, Gray NS, Knapp S. The ins and outs of selective kinase inhibitor development. Nature chemical biology. 2015; 11:818–821. [PubMed: 26485069]

19. Dolan BM, Duron SG, Campbell DA, Vollrath B, Shankaranarayana Rao BS, Ko HY, Lin GG, Govindarajan A, Choi SY, Tonegawa S. Rescue of fragile X syndrome phenotypes in Fmr1 KO mice by the small-molecule PAK inhibitor FRAX486. Proc Natl Acad Sci U S A. 2013; 110:5671–5676. [PubMed: 23509247]

20. Breitenlechner C, Gassel M, Hidaka H, Kinzel V, Huber R, Engh RA, Bossemeyer D. Protein kinase A in complex with Rho-kinase inhibitors Y-27632, Fasudil, and H-1152P: structural basis of selectivity. Structure. 2003; 11:1595–1607. [PubMed: 14656443]

21. Jacobs M, Hayakawa K, Swenson L, Bellon S, Fleming M, Taslimi P, Doran J. The structure of dimeric ROCK I reveals the mechanism for ligand selectivity. J Biol Chem. 2006; 281:260–268. [PubMed: 16249185]

22. Yamaguchi H, Kasa M, Amano M, Kaibuchi K, Hakoshima T. Molecular mechanism for the regulation of rho-kinase by dimerization and its inhibition by fasudil. Structure. 2006; 14:589–600. [PubMed: 16531242]

23. Bonn S, Herrero S, Breitenlechner CB, Erlbruch A, Lehmann W, Engh RA, Gassel M, Bossemeyer D. Structural analysis of protein kinase A mutants with Rho-kinase inhibitor specificity. J Biol Chem. 2006; 281:24818–24830. [PubMed: 16699172]

24. Heikkila T, Wheatley E, Crighton D, Schroder E, Boakes A, Kaye SJ, Mezna M, Pang L, Rushbrooke M, Turnbull A, Olson MF. Co-crystal structures of inhibitors with MRCKbeta, a key regulator of tumor cell invasion. PLoS One. 2011; 6:e24825. [PubMed: 21949762]

25. Licciulli S, Maksimoska J, Zhou C, Troutman S, Kota S, Liu Q, Duron S, Campbell D, Chernoff J, Field J, Marmorstein R, Kissil JL. FRAX597, a small molecule inhibitor of the p21-activated kinases, inhibits tumorigenesis of neurofibromatosis type 2 (NF2)-associated Schwannomas. J Biol Chem. 2013; 288:29105–29114. [PubMed: 23960073]

26. Rudolph J, Crawford JJ, Hoeflich KP, Chernoff J. p21-activated kinase inhibitors. The Enzymes. 2013; 34(Pt. B):157–180. [PubMed: 25034104]

27. Ndubaku CO, Crawford JJ, Drobnick J, Aliagas I, Campbell D, Dong P, Dornan LM, Duron S, Epler J, Gazzard L, Heise CE, Hoeflich KP, Jakubiak D, La H, Lee W, Lin B, Lyssikatos JP, Maksimoska J, Marmorstein R, Murray LJ, O'Brien T, Oh A, Ramaswamy S, Wang W, Zhao X, Zhong Y, Blackwood E, Rudolph J. Design of Selective PAK1 Inhibitor G-5555: Improving Properties by Employing an Unorthodox Low-pK a Polar Moiety. ACS medicinal chemistry letters. 2015; 6:1241–1246. [PubMed: 26713112]

28. Johnson LN. The regulation of protein phosphorylation. Biochem Soc Trans. 2009; 37:627–641. [PubMed: 19614568]

29. Teodoro ML, Phillips GN Jr, Kavraki LE. Understanding protein flexibility through dimensionality reduction. Journal of computational biology : a journal of computational molecular cell biology. 2003; 10:617–634. [PubMed: 12935348]

30. de Groot BL, Hayward S, van Aalten DM, Amadei A, Berendsen HJ. Domain motions in bacteriophage T4 lysozyme: a comparison between molecular dynamics and crystallographic data. Proteins. 1998; 31:116–127. [PubMed: 9593186]

31. Gorfe AA, Grant BJ, McCammon JA. Mapping the nucleotide and isoform-dependent structural and dynamical features of Ras proteins. Structure. 2008; 16:885–896. [PubMed: 18547521]

32. Yang L, Song G, Carriquiry A, Jernigan RL. Close correspondence between the motions from principal component analysis of multiple HIV-1 protease structures and elastic network modes. Structure. 2008; 16:321–330. [PubMed: 18275822]

33. Okazaki K, Takada S. Structural comparison of F1-ATPase: interplay among enzyme structures, catalysis, and rotations. Structure. 2011; 19:588–598. [PubMed: 21481781]
34. Kornev AP, Haste NM, Taylor SS, Eyck LF. Surface comparison of active and inactive protein kinases identifies a conserved activation mechanism. Proc Natl Acad Sci U S A. 2006; 103:17783–17788. [PubMed: 17095602]
35. Taylor SS, Shaw AS, Kannan N, Kornev AP. Integration of signaling in the kinome: Architecture and regulation of the alphaC Helix. Biochim Biophys Acta. 2015; 1854:1567–1574. [PubMed: 25891902]
36. Ryu BJ, Kim S, Min B, Kim KY, Lee JS, Park WJ, Lee H, Kim SH, Park S. Discovery and the structural basis of a novel p21-activated kinase 4 inhibitor. Cancer letters. 2014; 349:45–50. [PubMed: 24704155]
37. Park JK, Kim S, Han YJ, Kim SH, Kang NS, Lee H, Park S. The discovery and the structural basis of an imidazo[4,5-b]pyridine-based p21-activated kinase 4 inhibitor. Bioorg Med Chem Lett. 2016; 26:2580–2583. [PubMed: 27117431]
38. Martin MP, Alam R, Betzi S, Ingles DJ, Zhu JY, Schonbrunn E. A novel approach to the discovery of small-molecule ligands of CDK2. Chembiochem : a European journal of chemical biology. 2012; 13:2128–2136. [PubMed: 22893598]
39. Lawrie AM, Noble ME, Tunnah P, Brown NR, Johnson LN, Endicott JA. Protein kinase inhibition by staurosporine revealed in details of the molecular interaction with CDK2. Nat Struct Biol. 1997; 4:796–801. [PubMed: 9334743]
40. Abo A, Qu J, Cammarano MS, Dan C, Fritsch A, Baud V, Belisle B, Minden A. PAK4, a novel effector for Cdc42Hs, is implicated in the reorganization of the actin cytoskeleton and in the formation of filopodia. Embo J. 1998; 17:6527–6540. [PubMed: 9822598]
41. Baskaran Y, Ang KC, Anekal PV, Chan WL, Grimes JM, Manser E, Robinson RC. An in cellulo-derived structure of PAK4 in complex with its inhibitor Inka1. Nature communications. 2015; 6:8681.
42. Meyer PA, Socias S, Key J, Ransey E, Tjon EC, Buschiazzo A, Lei M, Botka C, Withrow J, Neau D, Rajashankar K, Anderson KS, Baxter RH, Blacklow SC, Boggon TJ, Bonvin AM, Borek D, Brett TJ, Caflisch A, Chang CI, Chazin WJ, Corbett KD, Cosgrove MS, Crosson S, Dhe-Paganon S, Cera E Di, Drennan CL, Eck MJ, Eichman BF, Fan QR, Ferre-D'Amare AR, Fromme JC, Garcia KC, Gaudet R, Gong P, Harrison SC, Heldwein EE, Jia Z, Keenan RJ, Kruse AC, Kvansakul M, McLellan JS, Modis Y, Nam Y, Otwinowski Z, Pai EF, Pereira PJ, Petosa C, Raman CS, Rapoport TA, Roll-Mecak A, Rosen MK, Rudenko G, Schlessinger J, Schwartz TU, Shamoo Y, Sondermann H, Tao YJ, Tolia NH, Tsodikov OV, Westover KD, Wu H, Foster I, Fraser JS, Maia FR, Gonen T, Kirchhausen T, Diederichs K, Crosas M, Sliz P. Data publication with the structural biology data grid supports live analysis. Nature communications. 2016; 7:10882.
43. Chen C, Ha BH, Thevenin AF, Lou HJ, Zhang R, Yip KY, Peterson JR, Gerstein M, Kim PM, Filippakopoulos P, Knapp S, Boggon TJ, Turk BE. Identification of a major determinant for serine-threonine kinase phosphoacceptor specificity. Mol Cell. 2014; 53:140–147. [PubMed: 24374310]
44. Otwinowski, Z., Minor, W. Processing of X-ray diffraction data collected in oscillation mode. In: Carter, CW., Sweet, RM., editors. Methods in Enzymology. Academic Press; New York; 1997. p. 307-326.Place Published
45. McCoy AJ. Solving structures of protein complexes by molecular replacement with Phaser. Acta Crystallogr D Biol Crystallogr. 2007; 63:32–41. [PubMed: 17164524]
46. Adams PD, Afonine PV, Bunkoczi G, Chen VB, Davis IW, Echols N, Headd JJ, Hung LW, Kapral GJ, Grosse-Kunstleve RW, McCoy AJ, Moriarty NW, Oeffner R, Read RJ, Richardson DC, Richardson JS, Terwilliger TC, Zwart PH. PHENIX: a comprehensive Python-based system for macromolecular structure solution. Acta Crystallogr D Biol Crystallogr. 2010; 66:213–221. [PubMed: 20124702]
47. Murshudov GN, Skubak P, Lebedev AA, Pannu NS, Steiner RA, Nicholls RA, Winn MD, Long F, Vagin AA. REFMAC5 for the refinement of macromolecular crystal structures. Acta Crystallogr D Biol Crystallogr. 2011; 67:355–367. [PubMed: 21460454]
48. Emsley P, Lohkamp B, Scott WG, Cowtan K. Features and development of Coot. Acta Crystallogr D Biol Crystallogr. 2010; 66:486–501. [PubMed: 20383002]

49. Schuttelkopf AW, van Aalten DM. PRODRG: a tool for high-throughput crystallography of protein-ligand complexes. Acta Crystallogr D Biol Crystallogr. 2004; 60:1355–1363. [PubMed: 15272157]
50. Chen VB, Arendall WB 3rd, Headd JJ, Keedy DA, Immormino RM, Kapral GJ, Murray LW, Richardson JS, Richardson DC. MolProbity: all-atom structure validation for macromolecular crystallography. Acta Crystallogr D Biol Crystallogr. 2010; 66:12–21. [PubMed: 20057044]
51. Morin A, Eisenbraun B, Key J, Sanschagrin PC, Timony MA, Ottaviano M, Sliz P. Cutting edge: Collaboration gets the most out of software. eLife. 2013; 2:e01456. [PubMed: 24040512]
52. McNicholas S, Potterton E, Wilson KS, Noble ME. Presenting your structures: the CCP4mg molecular-graphics software. Acta Crystallogr D Biol Crystallogr. 2011; 67:386–394. [PubMed: 21460457]
53. Eswaran J, Lee WH, Debreczeni JE, Filippakopoulos P, Turnbull A, Fedorov O, Deacon SW, Peterson JR, Knapp S. Crystal Structures of the p21-activated kinases PAK4, PAK5, and PAK6 reveal catalytic domain plasticity of active group II PAKs. Structure. 2007; 15:201–213. [PubMed: 17292838]
54. Murray BW, Guo C, Piraino J, Westwick JK, Zhang C, Lamerdin J, Dagostino E, Knighton D, Loi CM, Zager M, Kraynov E, Popoff I, Christensen JG, Martinez R, Kephart SE, Marakovits J, Karlicek S, Bergqvist S, Smeal T. Small-molecule p21-activated kinase inhibitor PF-3758309 is a potent inhibitor of oncogenic signaling and tumor growth. Proc Natl Acad Sci U S A. 2010; 107:9446–9451. [PubMed: 20439741]
55. Guo C, McAlpine I, Zhang J, Knighton DD, Kephart S, Johnson MC, Li H, Bouzida D, Yang A, Dong L, Marakovits J, Tikhe J, Richardson P, Guo LC, Kania R, Edwards MP, Kraynov E, Christensen J, Piraino J, Lee J, Dagostino E, Del-Carmen C, Deng YL, Smeal T, Murray BW. Discovery of pyrroloaminopyrazoles as novel PAK inhibitors. J Med Chem. 2012; 55:4728–4739. [PubMed: 22554206]
56. Crawford JJ, Lee W, Aliagas I, Mathieu S, Hoeflich KP, Zhou W, Wang W, Rouge L, Murray L, La H, Liu N, Fan PW, Cheong J, Heise CE, Ramaswamy S, Mintzer R, Liu Y, Chao Q, Rudolph J. Structure-Guided Design of Group I Selective p21-Activated Kinase Inhibitors. J Med Chem. 2015; 58:5121–5136. [PubMed: 26030457]
57. Kleywegt GJ. Validation of protein models from Calpha coordinates alone. J Mol Biol. 1997; 273:371–376. [PubMed: 9344745]
58. Edgar RC. MUSCLE: a multiple sequence alignment method with reduced time and space complexity. BMC Bioinformatics. 2004; 5:113. [PubMed: 15318951]
59. Theobald DL, Wuttke DS. Accurate structural correlations from maximum likelihood superpositions. PLoS computational biology. 2008; 4:e43. [PubMed: 18282091]
60. Skjaerven L, Yao XQ, Scarabelli G, Grant BJ. Integrating protein structural dynamics and evolutionary analysis with Bio3D. BMC Bioinformatics. 2014; 15:399. [PubMed: 25491031]
61. Stierand K, Rarey M. Drawing the PDB: Protein-Ligand Complexes in Two Dimensions. ACS medicinal chemistry letters. 2010; 1:540–545. [PubMed: 24900245]

AUTHOR SUMMARY

Protein kinases are key signaling proteins, and are important drug targets, therefore understanding their regulation is important for both basic research and clinical points of view. In this study, we observe unusual conformational ‘hinging’ for protein kinases. Hinging, the opening and closing of the kinase sub-domains to allow nucleotide binding and release, is critical for proper kinase regulation and for targeted drug discovery. We determine new crystal structures of PAK4, an important Rho-effector kinase, and conduct analyses of these and previously determined structures. We find that PAK4 crystal structures can be classified into specific conformational groups, and that these groups are associated with previously unobserved hinging motions and an unusual conformation for the kinase hydrophobic core. Our findings therefore indicate that there may be a diversity of kinase hinging motions, and that these may indicate different mechanisms of regulation.

HIGHLIGHTS

- Three crystal structures of PAK4 in complex with fasudil, FRAX486 and staurosporine.
- Principal component analysis reveals structural classes for PAK4 crystal structures.
- Disrupted R-spine indicated for inhibited state and an accessible back pocket cavity.
- Implies a diversity of kinase conformational changes potentially associated with regulation.

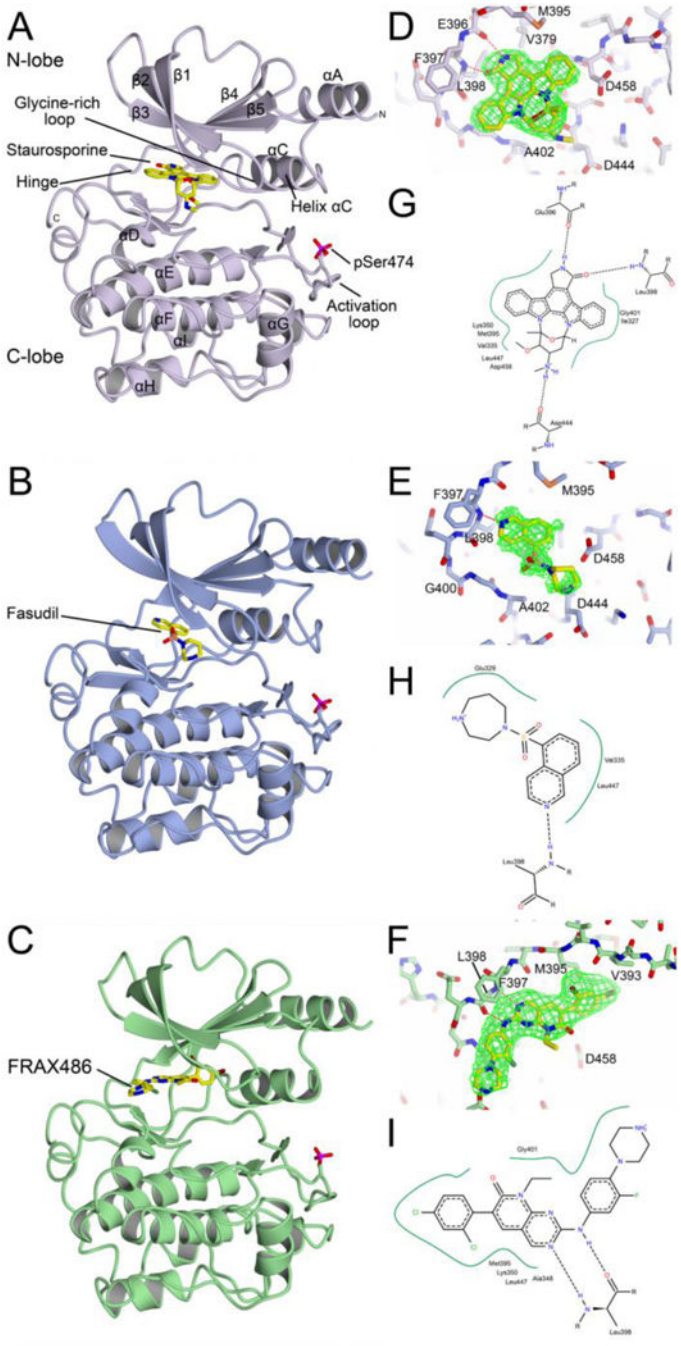

Figure 1. Crystal structures of PAK4 in complex with staurosporine, fasudil and FRAX486.

A,B,C) Overall structures showing bound small molecule in stick format. Secondary structure elements and kinase features are indicated. **D,E,F)** Detailed interactions of small molecules with PAK4. Hydrogen-bonds shown as red lines. Residues of interest indicated. *F*o-*F*c map for the final un-biased round of refinement before adding ligand shown in 2σ (light green) and 3σ (olive). **G,H,I)** Schematic of small molecule-PAK4 Interactions shown in PoseView format with van der Waals contacts indicated by a green line[61].

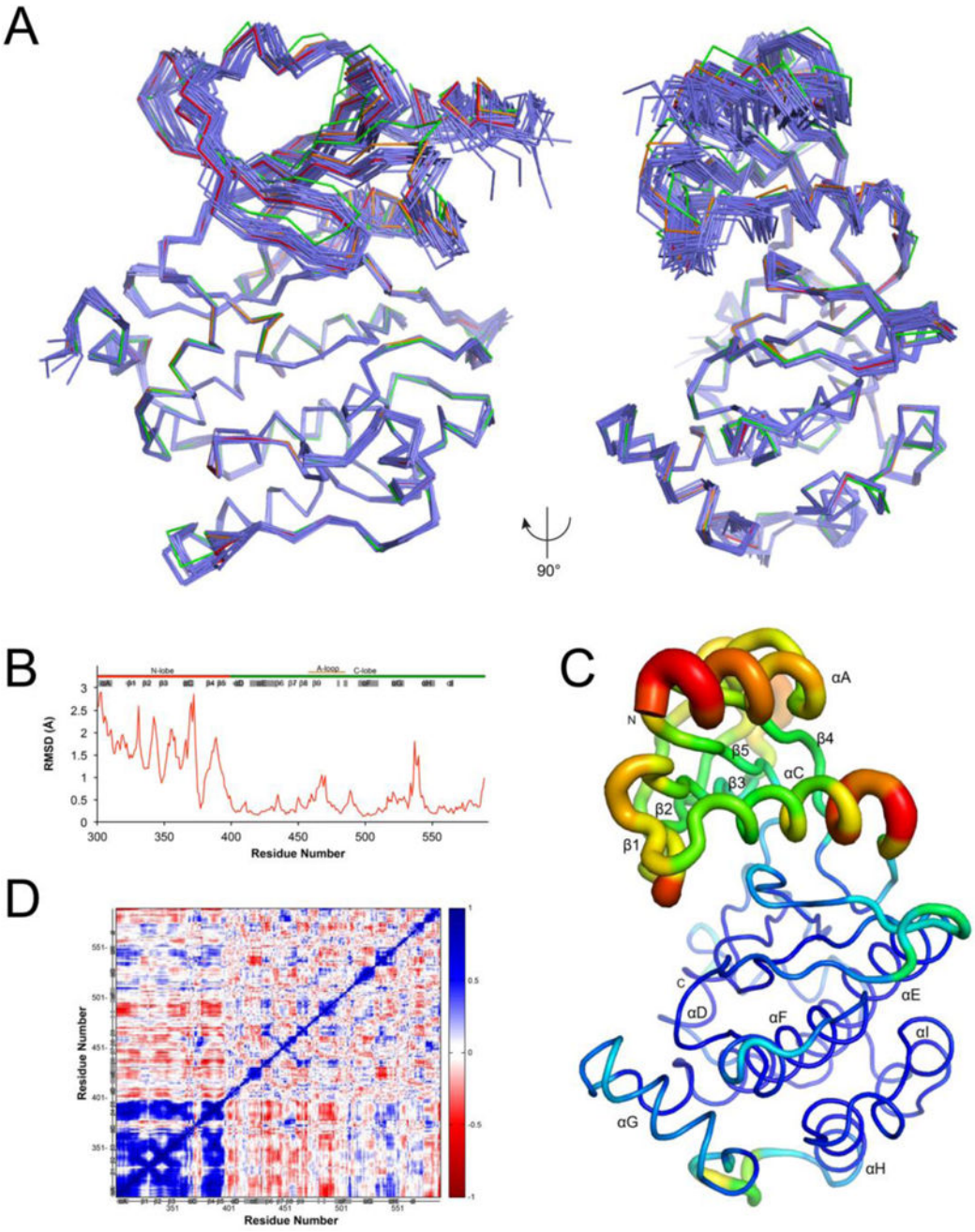

Figure 2. Comparison of all deposited PAK4 structures. A) Superposition onto the PAK4 C-lobe of the PAK4 catalytic domains described in this work (staurosporine, orange; fasudil, red; FRAX486, green) and previously deposited in the Protein Data Bank (PDB IDs: 2CDZ, 2J0I [53], 2Q0N, 4JDH, 4JDI, 4JDJ, 4JDK [43], 2X4Z [54], 4APP [55], 4FIE, 4FIF, 4FIG, 4FIH, 4FII, 4FIJ [10], 4L67 [12], 4NJD [36], 4O0V, 4O0X, 4O0Y [17], 4XBR, 4XBU [41], 5BMS [56], 5I0B [37] in blue. **B, C)** Root-mean-square deviation (RMSD) by residue number across all PAK4 structures. Calculated using Theseus[59] and shown using putty format on the structure of PAK4 with fasudil. **D)** Cross

correlation matrix calculated using Theseus[59]. Positive correlation is colored blue, negative correlation is colored red, and no correlation in white.

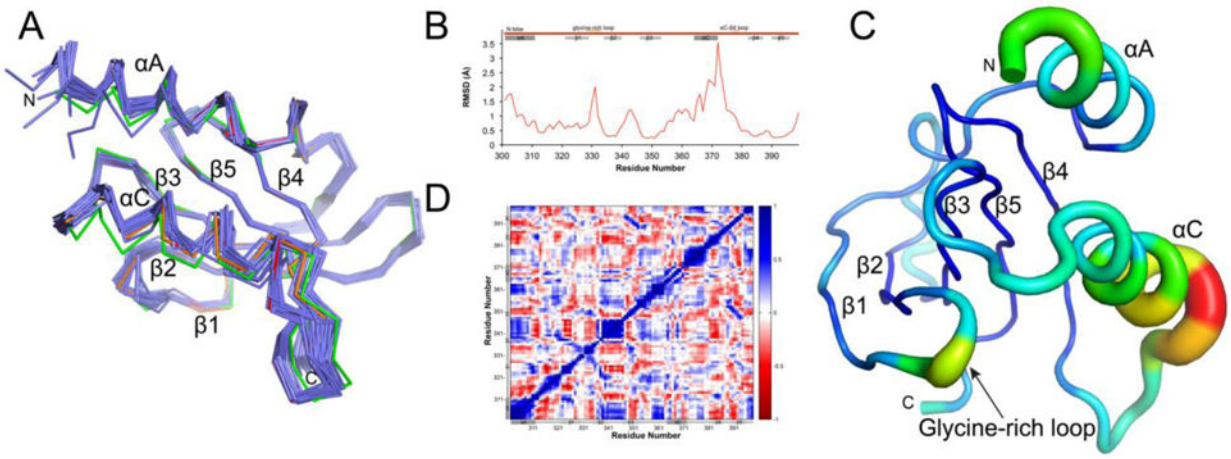

Figure 3. Assessment of the N-lobe for all deposited structures of PAK4. A) Superposition of the PAK4 N-lobe. PAK4 structures described in this work (staurosporine, orange; fasudil, red; FRAX486, green) and previously deposited in the PDB (PDB IDs: 2CDZ, 2J0I [53], 2Q0N, 4JDH, 4JDI, 4JDJ, 4JDK [43], 2X4Z [54], 4APP [55], 4FIE, 4FIF, 4FIG, 4FIH, 4FII, 4FIJ [10], 4L67 [12], 4NJD [36], 4O0V, 4O0X, 4O0Y [17], 4XBR, 4XBU [41], 5BMS [56], 5I0B [37] in blue. **B, C)** Root-mean-square deviation (RMSD) by residue number, calculated using Theseus[59] and shown using putty format on the structure of PAK4 with fasudil. **D)** Cross correlation matrix generated using Theseus[59]. Positive correlation is colored blue, negative correlation is colored red, and no correlation in white.

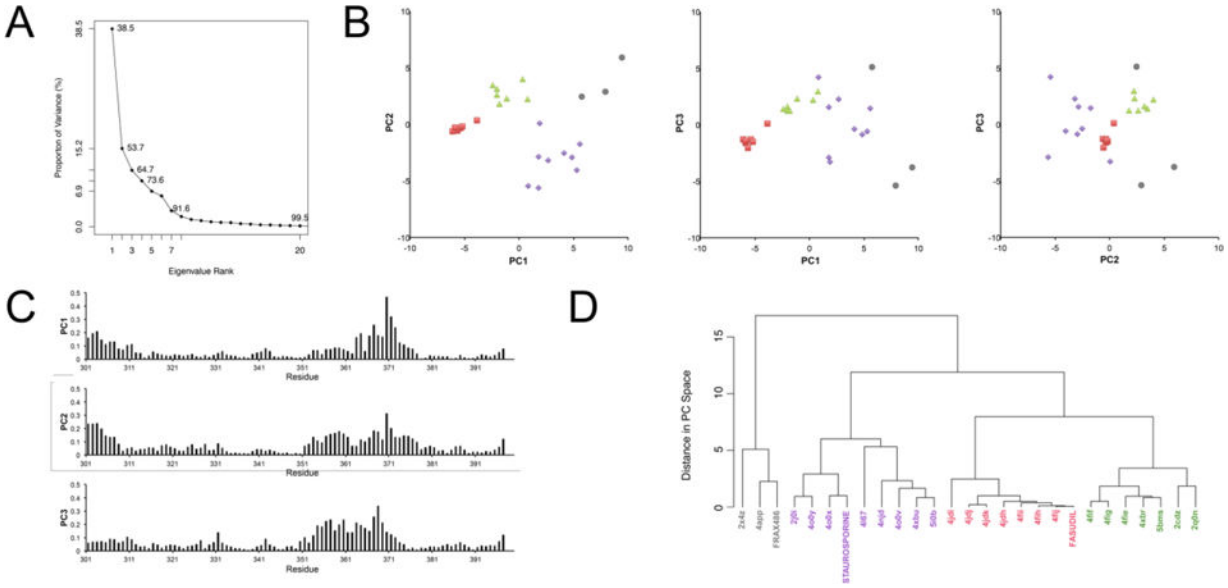

Figure 4. Principal component analysis for PAK4 N-lobes

Principal component analysis for the N-lobes (residues 301–399) of PAK4 structures PDB IDs: 2BVA, 2J0I [53], 2Q0N, 4JDH, 4JDI, 4JDJ, 4JDK [43], 2X4Z [54], 4APP [55], 4FIE, 4FIF, 4FIG, 4FIH, 4FII, 4FIJ [10], 4L67 [12], 4NJD [36], 4O0V, 4O0X, 4O0Y [17], 4XBR, 4XBU [41], 5BMS [56], 5I0B [37]. **A)** Eigenvalue contribution of the first 20 principal components from PCA. **B)** Mapping of the first 3 principal components, PC1, PC2 and PC3 for each structure. Left, PC2 vs PC1; center, PC3 vs PC1; right, PC3 vs PC2. Each dot represents a structure. Colors are indicated by cluster in panel D. **C)** Each residue's contribution to the first three principal components. **D)** Dendrogram of distances of PC space for principal components 1 and 2.

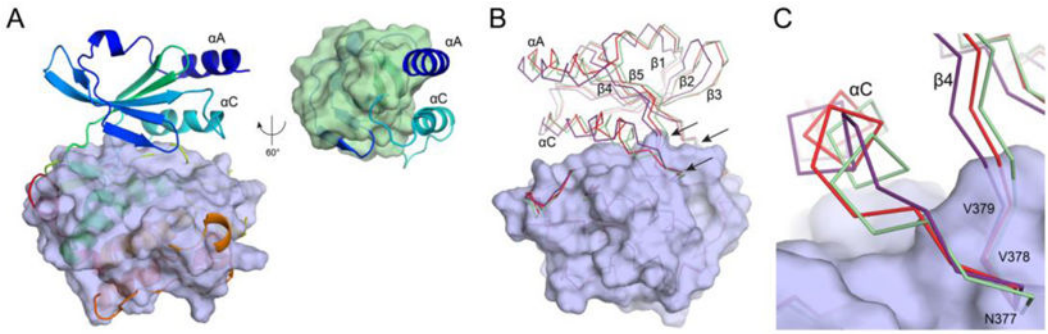

Figure 5. Rigid core of PAK4 based on RMSD analysis. A)
Rigid core of the whole catalytic domain (residues 301–589) on left, and N-lobe (residues 301–399) on right. PAK4 in complex with fasudil shown. Structure colored in Jones rainbow format. Cores shown as a transparent surface. **B)** Arrows indicate locations of N-lobe residues that are part of the rigid core for the whole domain. Conformational movements of the N-lobe do not affect these residues (in the hinge region and at the tip of the αC-β4 loop). Backbone trace for typical examples of the back-pocket-accessible (left, purple, PDB ID: 4XBU), ATP-bound-like (middle, green, PDB ID: 4FIF), and substrate-bound-like (right, red, PDB ID: 4JDJ) conformations. Selected secondary structure elements indicated. Rigid core of the whole catalytic domain shown as a transparent surface. **C)** Close up showing unwinding of helix αC and the location of residues Asn377, Val378 and Val379.

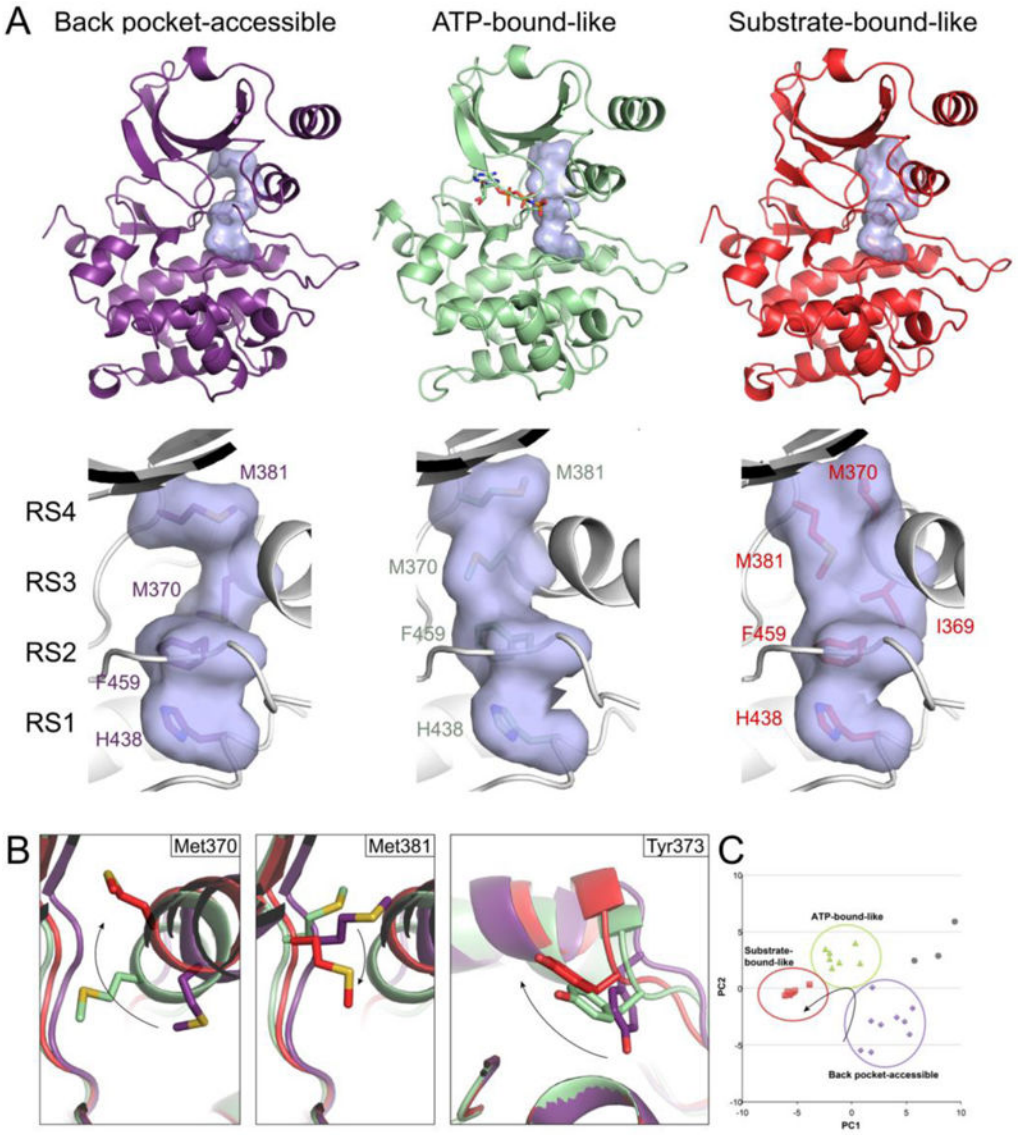

Figure 6. A potential trajectory of conformational movement in PAK4. A) R-spine analysis for typical examples of the back-pocket-accessible (left, purple, PDB ID: 4XBU), ATP-bound-like (middle, green, PDB ID: 4FIF), and substrate-bound-like (right, red, PDB ID: 4JDJ) conformations. Top row is overall view, bottom row is a close up. R-spine positions RS1-RS4 are indicated. Structures shown **B)** Close up views of specific residues indicated. **C)** Proposed trajectory plotted onto a map of the first two principal components for the kinase N-lobe (as plotted in Fig 4B).

Table 1

Data collection and refinement statistics.

Complex	**PAK4-staurosporine**	**PAK4-fasudil**	**PAK4-FRAX486**
PDB accession code	**5VED**	**5VEF**	**5VEE**
Data Collection			
Space group	$P4_12_12$	$P4_12_12$	$P4_12_12$
X-ray source	APS, 24-ID-E	APS, 24-ID-E	APS, 24-ID-E
Number crystals	1	1	1
Cell a, b, c (Å)	62.7, 62.7, 177.2	61.9, 61.9, 182.7	63.0, 63.0, 183.5
α, β, γ (°)	90, 90, 90	90, 90, 90	90, 90, 90
Wavelength (Å)	0.97919	0.97919	0.97919
Resolution range (Å) *	50 – 2.30 (2.38 – 2.30)	50 – 1.75 (1.81 – 1.75)	50 – 2.50 (2.59 – 2.50)
No. unique reflections	16,575 (1,608)	35,807 (3,297)	13,760 (1,313)
Degrees of data (°)	180	180	180
Completeness (%) *	100 (100)	97.0 (91.4)	99.9 (100)
R_{pim} (%) *	8.9 (94.6)	3.1 (70.9)	2.1 (83.5)
$I / \sigma I$ *	8.0 (1.4)	20.4 (1.6)	23.1 (1.4)
Redundancy *	12.8 (12.9)	12.2 (10.4)	20.1 (13.5)
Wilson B-factor (Å^2)	43.2	27.7	88.0
Refinement			
Resolution range (Å) *	43.0 – 2.30 (2.45 – 2.30)	43.8 – 1.75 (1.80 – 1.75)	43.9 – 2.50 (2.57 – 2.50)
R_{factor} (%) *	22.8 (34.9)	20.0 (29.9)	22.8 (46.8)
Free R_{factor} (%) *	27.7 (39.2)	23.9 (31.6)	27.6 (46.5)
No. Free R reflections *	886 (154)	1733 (118)	704 (45)
Residue range built	300–589	300–589	300–589
No. water molecules	15	136	0
Model Quality			
RMSD bond lengths (Å)	0.002	0.008	0.013
RMSD bond angles (o)	0.550	1.080	1.691
Overall B (all atoms) (Å^2)	52.4	42.6	115.6
B (Å^2) protein/water/ligand	52.6 / 42.4 / 39.2	42.2 / 40.3 / 110.2	117.6 / – / 92.2
Ramachandran plot (%) favored/allowed/outliers	96.2 / 3.8 / 0.0	98.6 / 1.4 / 0.0	90.6 / 9.4 / 0.0
MolProbity score/percentile	3.19 / 100%	0.85 / 100%	4.06 / 99%

* Parentheses indicate highest resolution shell

Biochim Biophys Acta. Author manuscript; available in PMC 2019 February 01.

Table 2

Summary of Principal Component Analysis

PCA analysis for residues 301–589 (catalytic domain) and 301–399 (N-lobe). Built peptide types are “subst” for substrate and “pseudo” for pseudosubstrate inhibitor. PDB Chain IDs are colored as per PCA classifications in Figure 5. Citations are [10, 12, 17, 36, 37, 41, 43, 53–56]. Structure 2BVA was not included in the PCA analysis because of multiple unbuilt residues. PCA defined conformational classes indicated: ATP-bound-like conformation (ATP), substrate-bound-like conformation (SUB), inhibitor-accessible-only conformations (INH), and back pocket-accessible cavity (CAV).

PDB ID	Built inhibitor nucleotide visible	PDB ligand identifier	Built peptide type	PCA class	Resoluti on	PCA for catalytic domain			PCA for N-lobe			Citation
						PC1	PC2	PC3	PC1	PC2	PC3	
2BVA	–	–	–	–	2.3	Not included			Not included			Eswaran *et al.*, 2007
2CDZ	CGP74514A	23D	–	ATP	2.3	2.3	5.8	−5.3	0.8	2.2	3.0	Eswaran *et al.*, 2007
2J0I	–	–	–	CAV	1.6	17.1	−2.6	2.3	1.8	−5.6	−2.9	Eswaran *et al.*, 2007
2Q0N	–	–	subst	ATP	1.75	1.9	8.7	−8.4	0.3	4.0	2.2	Chen *et al.*, 2014
2X4Z	PF-03758309	X4Z	–	INH	2.1	−6.3	3.0	13.2	9.5	5.9	−3.8	Murray *et al.*, 2010
4APP	Compound 3	N53	–	INH	2.2	3.1	1.3	7.1	7.9	2.9	−5.4	Guo *et al.*, 2012
4FIE	AMP-PNP	ANP	pseudo	ATP	3.11	−10.0	3.8	−4.7	−2.0	2.6	1.2	Ha *et al.*, 2012
4FIF	ANP-PNP	ANP	pseudo	ATP	2.6	−11.6	5.0	−4.8	−2.4	3.5	1.4	Ha *et al.*, 2012
4FIG	ANP-PNP	ANP	–	ATP	3.01	−13.1	5.0	−3.4	−2.0	3.2	1.6	Ha *et al.*, 2012
4FIH	–	–	–	SUB	1.97	0.8	−10.2	−1.8	−5.9	−0.3	−1.6	Ha *et al.*, 2012
4FII	–	–	pseudo	SUB	2.0	1.0	−10.0	−2.6	−5.6	−0.6	−2.1	Ha *et al.*, 2012
4FIJ	–	–	–	SUB	2.3	0.7	−9.6	−1.8	−5.8	−0.3	−1.5	Ha *et al.*, 2012
4JDH	–	–	subst	SUB	2.0	−3.0	−10.7	0.3	−6.1	−0.6	−1.3	Chen *et al.*, 2014
4JDI	AMP-PNP	ANP	subst	SUB	1.85	−0.8	−7.2	−0.8	−3.9	0.4	0.1	Chen *et al.*, 2014
4JDJ	–	–	subst	SUB	2.3	0.0	−8.4	−1.6	−5.3	−0.4	−1.3	Chen *et al.*, 2014
4JDK	–	–	subst	SUB	2.4	−1.3	−9.0	−0.9	−5.2	−0.2	−1.5	Chen *et al.*, 2014
4L67	–	–	pseudo	CAV	2.8	5.7	3.0	−1.8	1.9	0.1	−3.3	Wang *et al.*, 2013
4NJD	KY-04031	NJD	–	CAV	2.5	14.0	7.5	1.6	5.3	−4.0	−0.6	Ryu *et al.*, 2014
4O0V	Compound 17	2OL	–	CAV	2.8	3.4	7.1	3.9	5.6	−1.8	1.4	Staben *et al.*, 2014
4O0X	Compound 8	2OQ	–	CAV	2.48	3.7	4.1	1.1	2.7	−3.2	2.3	Staben *et al.*, 2014
4O0Y	Compound 13	2O0	–	CAV	2.2	1.9	2.5	0.4	0.8	−5.4	4.2	Staben *et al.*, 2014

PDB ID	Built inhibitor nucleotide visible	PDB ligand identifier	Built peptide type	PCA class	Res oluti on	PCA for catalytic domain			PCA for N-lobe			Citation
4XBR	ATP	ATP	–	ATP	2.94	−10.1	7.9	−4.3	−1.8	1.8	1.2	Baskaran *et al.*, 2015
4XBU	–	–	pseudo	CAV	2.06	11.8	6.3	−0.1	4.9	−2.9	−0.9	Baskaran *et al.*, 2015
5BMS	Compound 29	4T6	–	ATP	2.9	−5.4	−0.8	−0.6	−1.1	2.3	2.3	Crawford *et al.*, 2015
5I0B	KY-04045	67U	–	CAV	3.09	11.0	6.9	−1.5	4.1	−2.5	−0.4	Park *et al.*, 2016
5VED	Staurosporine	STU	–	CAV	2.3	−2.5	−4.2	6.6	1.8	−2.9	1.6	This study
5VEF	Fasudil	M77	–	SUB	1.75	0.4	−10.7	−1.3	−5.8	−0.3	−1.4	This study
5VEE	FRAX486	FRA	–	INH	2.5	−14.4	5.6	9.4	5.7	2.4	5.1	This study